BNL-NT-05/51

THE DENSITY OF STATES METHOD AT FINITE CHEMICAL POTENTIAL

Christian Schmidt[*1], *Zoltan Fodor*[2,3] *and Sandor Katz*[3]
[1] Physics Department, Brookhaven National Laboratory, Bldg. 510A, Upton, NY, 11973, USA
[2] Department of Physics, University of Wuppertal, Gaussstrasse 20, D-42119, Germany
[3] Institute for Theoretical Physics, Eötvös University, Pazmany 1, H-1117 Budapest, Hungary

Abstract
We study the density of states method to explore the phase diagram of the chiral transition on the temperature and quark chemical potential plane. Four quark flavors are used in the analysis. Though the method is quite expensive small lattices show an indication for a triple-point connecting three different phases on the phase diagram.

1 Introduction

To clarify the phase diagram of QCD and thus the nature of matter under extreme conditions is one of the most interesting and fundamental tasks of high energy physics. Lattice QCD has been shown to provide important and reliable information from first principals on QCD at zero density. However, Lattice QCD at finite densities has been harmed by the complex action problem ever since its inception. For $\mu > 0$ the determinant of the fermion matrix (detM) becomes complex. Standard Monte Carlo techniques using importance sampling are thus no longer applicable when calculating observables in the grand canonical ensemble according to the partition function

$$Z_{GC}(\mu) = \int \mathcal{D}U \ \mathrm{detM[U]}(\mu) \exp\{-\mathrm{S_G[U]}\}. \tag{1}$$

Recently many different methods have been developed to circumvent the complex action problem for small μ/T [1, 2]. For a recent overview see also [3].

2 Formulation of the method

A very general formulation of the DOS method is the following: One exposed parameter (ϕ) is fixed. The expectation value of a thermodynamic observable (O), according to the usual grand canonical partition function (1), can be recovered by the integral

$$< O >= \int d\phi \ \langle O f(U) \rangle_\phi \, \rho(\phi) \Big/ \int d\phi \ \langle f(U) \rangle_\phi \, \rho(\phi) \tag{2}$$

where the density of states (ρ) is given by the constrained partition function:

$$\rho(x) \equiv Z_\phi(x) = \int \mathcal{D}U \, g(U) \, \delta(\phi - x). \tag{3}$$

With $\langle \ \rangle_\phi$ we denote the expectation value with respect to the constrained partition function. In addition, the product of the weight functions f, g has to give the correct measure of Z_{GC}: $fg = \mathrm{detM} \exp\{-\mathrm{S_G}\}$. This idea of reordering the partition functions is rather old and was used in many different cases [4, 5, 6] The advantages of this additional integration becomes clear, when choosing $\phi = P$ and $g(U) = 1$. In this case $\rho(\phi)$ is independent of all simulation parameters. The observable can be calculated as a function of all values of the lattice coupling β. If one has stored all eigenvalues of the fermion matrix for all

[*] Speaker

configurations, the observable can also be calculated as a function of quark mass (m) and number of flavors[5] (N_f). In this work we chose

$$\phi = P \qquad \text{and} \qquad g = |\det M| \exp\{-S_G\}, \qquad f = \exp\{i\theta\}. \tag{4}$$

In other words we constrain the plaquette and perform simulations with measure g. In practice, we replace the delta function in Equation (3) by a sharply peaked potential [6]. The constrained partition function for fixed values of the plaquette expectation value can then be written as

$$\rho(x) \approx \int \mathcal{D}U \; g(U) \exp\left\{-V(x)\right\}, \tag{5}$$

where $\exp\{-V(x)\}$ is a Gaussian potential with

$$V(x) = \frac{1}{2}\gamma \left(x - P\right)^2. \tag{6}$$

We obtain the density of states ($\rho(x)$) by the fluctuations of the actual plaquette P around the constraint value x. The fluctuation dissipation theorem gives

$$\frac{d}{dx} \ln \rho(x) =< x - P >_x . \tag{7}$$

Before performing the integrals in Equation (2) we compute from an ensemble generated at (μ_0, β_0):

$$\langle Of(U)\rangle_x (\mu, \beta) = \langle Of(U) R(\mu, \mu_0, \beta, \beta_0)\rangle_x \,/\, \langle R(\mu, \mu_0, \beta, \beta_0)\rangle_x , \tag{8}$$

$$\langle f(U)\rangle_x (\mu, \beta) = \langle f(U) R(\mu, \mu_0, \beta, \beta_0)\rangle_x \,/\, \langle R(\mu, \mu_0, \beta, \beta_0)\rangle_x , \tag{9}$$

$$\frac{d}{dx} \ln \rho(x, \mu, \beta) = \langle (x - P) R(\mu, \mu_0, \beta, \beta_0)\rangle_x . \tag{10}$$

Here R is given by the quotient of the measure g at the point (μ, β) and at the simulation point (μ_0, β_0),

$$R(\mu, \mu_0, \beta, \beta_0) = g(\mu, \beta)/g(\mu_0, \beta_0) = \frac{|\det(\mu)|}{|\det(\mu_0)|} \exp\{S_G(\beta) - S_G(\beta_0)\}. \tag{11}$$

Having calculated the expressions (8)-(10), we are able to extrapolate the expectation value of the observable (2) to any point (μ, β) in a small region around the simulation point (μ_0, β_0). For any evaluation of $\langle O\rangle (\mu, \beta)$, we numerically perform the integrals in Equation (2). We also combine the data from several simulation points to interpolate between them.

3 Simulations with constrained Plaquette

The value we want to constrain is the expectation value of the global plaquette, which is given on every gauge configuration by the sum over all lattice points (y) and directions ($\mu\nu$) of the local plaquette $P_{\mu\nu}(y)$ and its adjoint $P^\dagger_{\mu\nu}(y)$,

$$P = \sum_y \sum_{1 \le \mu < \nu \le 4} \frac{1}{6} \left[\mathrm{Tr} P_{\mu\nu}(y) + \mathrm{Tr} P^\dagger_{\mu\nu}(y) \right]. \tag{12}$$

Since the plaquette is also the main part of the gauge action,

$$S_G = -\beta \sum_x \sum_{1 \le \mu < \nu \le 4} \left\{ \frac{1}{6} \left[\mathrm{Tr} P_{\mu\nu}(x) + \mathrm{Tr} P^\dagger_{\mu\nu}(x) \right] - 1 \right\}, \tag{13}$$

the additional potential V can be easily introduced in the hybrid Monte Carlo update procedure of the hybrid-R algorithm [7]. After calculating the equation of motion for the link variables $U_\mu(y)$, we find for the gauge part of the force

$$i\dot{H}_\mu(y) = \left[\frac{\beta}{3} U_\mu(y) T_\mu(y) \left(1 + \frac{\gamma(x - P)}{\beta} \right) \right]_{\mathrm{TA}} . \tag{14}$$

Here the subscript TA indicates the traceless anti-Hermitian part of the matrix. We see that in each molecular dynamical step the measurement of the plaquette is required. However, the only modification in the gauge force is the factor in round brackets.

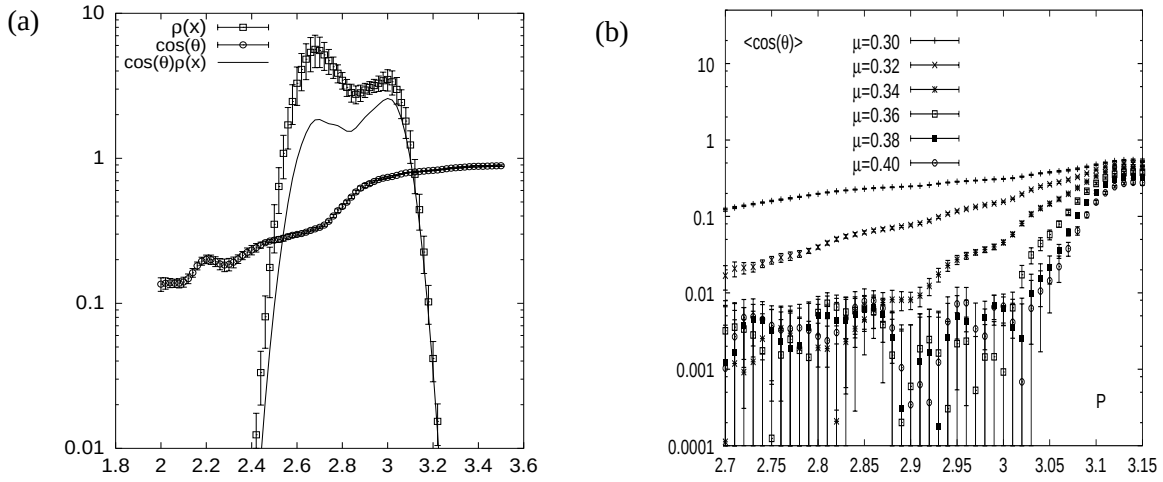

Fig. 1: (a) Results for Simulations at $\beta = 4.98$, $\mu = 0.3$, $\lambda = 0.02$, $n_f = 4$, $am = 0.05$, and number of lattice points: 4^4. Shown are the density of states $\rho(x)$, the phase factor $\langle \cos(\theta) \rangle$, and their product. (b) Results for Simulations at $\beta = 5.1$, $\lambda = 0.01$, $n_f = 4$, $am = 0.05$, and number of lattice points: 6^4. Shown is the suppression from the complex phase of the fermion determinant $\langle cos(\theta) \rangle$ for different chemical potentials.

4 Simulation details and the strength of the sign problem

Simulations have been performed with staggered fermions and $N_f = 4$. We chose 9 differed points in the (β, μ)-plane for the 4^4 lattice and 8 points for the 6^4 lattice. On each of these points we did simulations with 20-40 constrained plaquette values, all with quark mass $am = 0.05$. Further simulations has been done with $(\beta, \mu) = (5.1, 0.3)$ on the $6^3 \times 8$ lattice for $am = 0.05$ and $am = 0.03$. In order to calculate the plaquette expectation value, or its susceptibility, one has to perform the following integrals:

$$\langle P \rangle = \int dx \; x \rho(x) \left\langle cos(\theta) \right\rangle_x , \qquad \left\langle P^2 \right\rangle = \int dx \; x^2 \rho(x) \left\langle cos(\theta) \right\rangle_x . \tag{15}$$

Thus the functions $\rho(x)$ and $\left\langle cos(\theta) \right\rangle_x$ have to be known quite precisely. We plot both functions in Figure 1(a). The transition is signaled in the double peak structure of $\rho(x)$. The phase factor $\left\langle cos(\theta) \right\rangle_x$ suppresses the peak of $\rho(x)$ at smaller plaquette values, which results in a shift of the critical temperature to smaller values, in comparison with the phase quenched theory. In Figure 1(b) we show the phase factor for different chemical potentials. With increasing chemical potential the phase factor becomes compatible with zero within errors. In fact, its average value becomes as low as $cos(\theta) \sim 0.005$. There exist however a small interval around $P \sim 2.85$, where the phase factor stays finite. In this way, the Plaquette expectation values is strongly altered by the phase factor. Figure 1(b) demonstrates also the advantage of he DOS method over the other approaches of lattice QCD to finite density. Using the DOS method one is able to do simulations at directly those Plaquette values which are relevant at finite density. This solves the so called overlap problem of the reweighting approach. Furthermore we have checked in [8], that results with have been obtained within the framework of the DOS method agree very well with earlier results from the multi-reweighting approach.

5 The Plaquette expectation value and the phases diagram

Performing the integration in Eq. (15) numerically, we calculate the plaquette expectation values as shown in Fig. 2. At chemical potentials $\mu \lesssim 0.36$, the plaquette signals the QCD transition through a rapid crossover from a low temperature phase of $< P > \sim 2.9$ to a high temperature phase of $< P > \sim 3.1$. For $\mu \gtrsim 0.36$ the plaquette expectation value at small temperatures drops to $< P > \sim 2.85$. This new low temperature phase of the plaquette at high chemical potentials is caused by the fermion determinant.

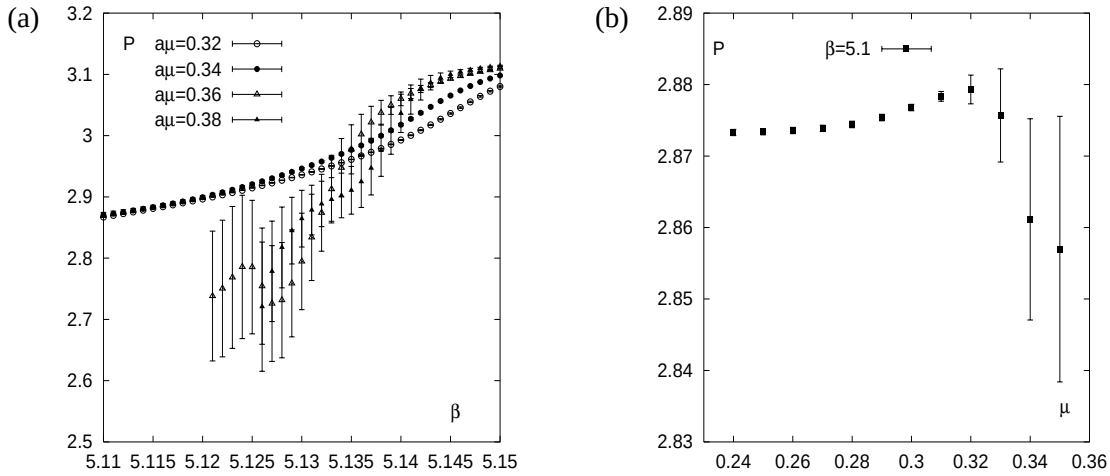

Fig. 2: Results for Simulations at $\beta = 5.1$, $\lambda = 0.01$, $n_f = 4$, $am = 0.05$, and number of lattice points: 6^4. Shown is: (a) the Plaquette expectation value as a function of the coupling β for different chemical potentials and (b) the plaquette expectation value at fixed coupling, as a function of the chemical potential.

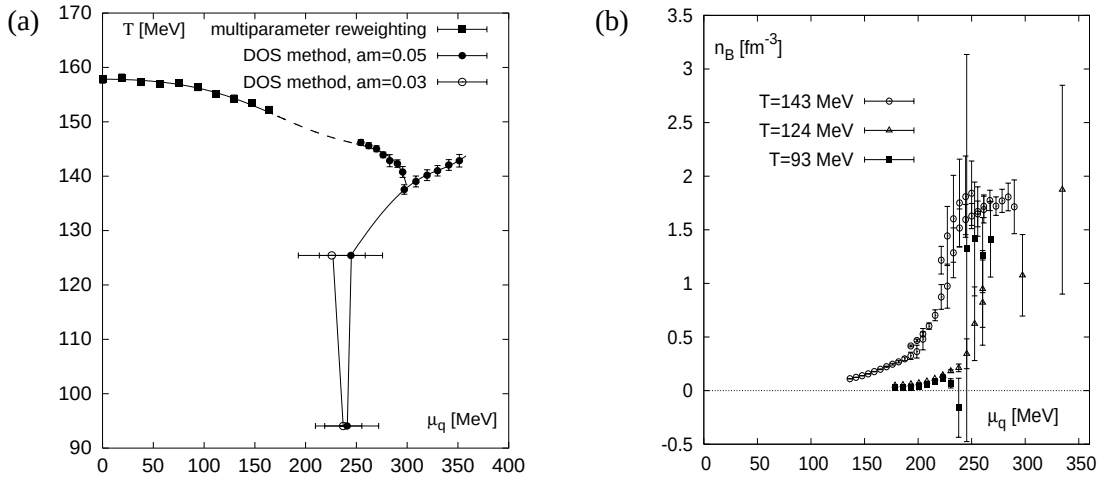

Fig. 3: The phase diagram in physical (a), and the quark number density at constant temperature $T = 143$ MeV (4^4 lattice), $T = 124$ MeV (6^4 lattice) and $T = 93$ MeV ($6^3 \times 8$ lattice).

As on can see in Figure 1(b) the region around $P \sim 2.85$ is the region which is less suppressed by the phase factor. Another interesting observation is that the critical coupling, which is decreasing in μ for $\mu < 0.36$ starts to increase for $\mu > 0.36$. The plaquette expectation value thus suggests the existence of three different phases in the (T,μ)-diagram with a triple point, where all those phases coincide. In Figure 3(a) we show the phase diagram in physical units. The phase boundaries were determined by calculating the peaks in the plaquette susceptibility. Note, that we make no statement about the order of the transition lines. To determine the order of the transition one has to perform finite a finite-size-scaling analysis.

The scale was set by the Sommer radius r_0, measured on a $10^3 \times 20$ lattice. The triple point is located around $\mu_q^{\rm tri} \approx 300$ MeV, however its temperature ($T^{\rm tri}$) decreases from $T^{\rm tri} \approx 148$MeV on the 4^4 lattice to $T^{\rm tri} \approx 137$MeV on the 6^4 lattice. This shift reflects the relatively large cut-off effects one faces, with standard staggered fermions and temporal extents of 4 and 6.

Also shown in Figure 3(a) are points from simulations with quark mass $am = 0.03$. The phase boundary turned out to be — within our statistical uncertainties — independent of the the mass.

6 The quark number density

To reveal the properties of the new phase located in the lower right corner of the phase diagram, we calculated the quark number density, at constant coupling β and at constant temperature respectively. To obtain the density n_q we perform the following integration

$$\left\langle \frac{\mathrm{d}\ln\det M}{\mathrm{d}(a\mu)} \right\rangle = \int dx \left\langle \frac{\mathrm{d}\ln\det M}{\mathrm{d}(a\mu)} cos(\theta) \right\rangle_x \rho(x) \tag{16}$$

The thermodynamic quantity n_q are given as usual by

$$n_q = \frac{1}{a^3 N_s^3 N_t} \left\langle \frac{\mathrm{d}\ln\det M}{\mathrm{d}(a\mu)} \right\rangle \tag{17}$$

In Figure 3(b) we show the baryon number density, which is related to the quark number density by $n_B = n_q/3$. The results are plotted in physical units and correspond to a constant temperature of $T \approx 143$ MeV (4^4 lattice), $T \approx 124$ MeV (6^4 lattice) and $T \approx 93$ MeV ($6^4 \times 8$ lattice). In order to divide out the leading order cut-off effect, we multiply we have multiplied the data with the factor $c = SB(N_t)/SB$, which is the Stefan-Boltzmann value of a free lattice gas of quarks at a given value of N_t, divided by its continuum Stefan-Boltzmann value. At the same value of the chemical potential where we find also a peak in the susceptibility of the plaquette (μ_c), we see a sudden rise in the baryon number density. Thus for $\mu > \mu_c$ we enter a phase of dense matter. The transition occurs at a density of $(2-3) \times n_N$, where n_N denotes nuclear matter density. Above the transition, the density reaches values of $(10-20) \times n_N$. Quite similar results have been obtained recently by simulations in the canonical ensemble [9].

References

[1] Z. Fodor and S. D. Katz, *Phys. Lett.* **B534** (2002) 87 [hep-lat/0104001].

[2] Z. Fodor and S. D. Katz, *JHEP* **0203** (2002) 014; C. R. Allton *et al.*, *Phys. Rev.* **D66** (2002) 074507; R. V. Gavai and S. Gupta, *Phys. Rev.* **D 68** (2003) 034506; P. R. Crompton, [hep-lat/0301001]; M. D'Elia and M. P. Lombardo, *Phys. Rev.* **D67** (2003) 014505; P. de Forcrand and O. Philipsen, *Nucl. Phys.* **B642** (2002) 290; *Nucl. Phys.* **B673** (2003) 170; V. Azcotiti, *et al.*, [hep-lat/0503010].

[3] O. Philipsen, *PoS* **LAT2005** (2005) 016 [hep-lat/0510077].

[4] G. Bhanot, K. Bitar and R. Salvador, *Phys. Lett.* **B187** (1987) 381; *Phys. Lett.* **B188** (1987) 246; M. Karliner, S.R. Sharpe and Y.F. Chang, *Nucl. Phys.* **B302** (1988) 204; V. Azcoiti, G. di Carlo and A. F. Grillo, *Phys. Rev. Lett.* **65** (1990) 2239; A. Gocksch, *Phys. Rev. Lett.* **61** (1988) 2054.

[5] X. Q. Luo, *Mod. Phys. Lett.* **A16** (2001) 1615.

[6] J. Ambjorn, K. N. Anagnostopoulos, J. Nishimura and J. J. M. Verbaarschot, *JHEP* **0210** (2002) 062.

[7] S. Gottlieb, W. Liu, D. Toussaint, R. L. Renken and R. L. Sugar, *Phys. Rev.* **B35** (1987) 2531.

[8] C. Schmidt, Z. Fodor and S. Katz, *PoS* **LAT2005** (2005) 163 [hep-lat/0510087].

[9] A. Alexandru, M. Faber, I. Horvath and K. F. Liu, [hep-lat/0410002]; S. Kratochvila and P. de Forcrand, *PoS* **LAT2005** (2005) 167 [hep-lat/0509143].